Synthesis and Structure Characterization of Chromium Oxide Prepared by Solid Thermal Decomposition Reaction

Li Li,[†,‡] Zi F. Yan,*[,†] Gao Q. Lu,[‡] and Zhong H. Zhu[‡]

State Key Laboratory for Heavy Oil Processing, Key Laboratory of Catalysis, CNPC, China University of Petroleum, Dongying 257061, China, and ARC Centre for Functional Nanomaterials, School of Engineering, University of Queensland, QLD 4072, Australia

Received: July 12, 2005; In Final Form: October 16, 2005

Mesoporous chromium oxide (Cr_2O_3) nanocrystals were first synthesized by the thermal decomposition reaction of $Cr(NO_3)_3 \cdot 9H_2O$ using citric acid monohydrate (CA) as the mesoporous template agent. The texture and chemistry of chromium oxide nanocrystals were characterized by N_2 adsorption−desorption isotherms, FTIR, X-ray diffraction (XRD), UV−vis, and thermoanalytical methods. It was shown that the hydrate water and CA are the crucial factors in influencing the formation of mesoporous Cr_2O_3 nanocrystals in the mixture system. The decomposition of CA results in the formation of a mesoporous structure with wormlike pores. The hydrate water of the mixture provides surface hydroxyls that act as binders, making the nanocrystals aggregate. The pore structures and phases of chromium oxide are affected by the ratio of precursor-to-CA, thermal temperature, and time.

Introduction

Ultrafine nanostructured chromium(III) oxide with high surface areas has attracted considerable interest because of a wide variety of applications such as in green pigments, coating materials for thermal protection and wear resistance, heterogeneous catalysts, solar energy collectors, and transparent colorants, etc.[1−5] In catalysis, both chromium oxide and supported chromium have been used in many reactions such as polymerization,[6] dehydrogenation,[7−9] dehydrocyclization,[10,11] and selective catalytic reduction of NO_x with ammonia.[12−14] Various techniques have been developed to synthesize Cr_2O_3 nanoparticles such as precipitation,[15] precipitation−gelation,[16−18] sol−gel,[19−21] mechanochemical reaction, and subsequent heat treatment,[22] oxidation of chromium in oxygen,[23] and sonochemical methods.[24]

Recently, it has been reported that chromium hydroxide gels were precipitated from Cr $(NO_3)_3$ solutions by the addition of hydrazine monohydrate.[25] Hexagonal crystallites of Cr_2O_3 were obtained at 380 °C to 405 °C, the space group being $R\bar{3}c$. Hou et al. prepared Cr_2O_3 nanoparticles with crystallite sizes of 17−25 nm by evaporation of a $Cr(NO_3)_3$ solution.[26] However, the most efficient method for providing a large surface area is homogeneous precipitation, that is, slow alkalinization of an aqueous $Cr(NO_3)_3$ solution by hydrolysis of dissolved urea. The samples obtained by this method are microporous materials with a surface area of 250−350 $m^2 \cdot g^{-1}$, corresponding to a pore diameter of 0.6−2.0 nm. To prevent the collapse of the initial gel texture during the thermal treatment step, water was replaced by methanol, followed by supercritical release of the methanol at 305 °C. The produced mesoporous aerogels have high surface areas of about 503−785 $m^2 \cdot g^{-1}$, which correspond to a pore diameter of 20 nm.[27] Therefore, several groups reported the direct synthesis of highly crystalline and monodisperse metal oxide nanocrystals via the thermal decomposition of organometallic precursors.[28−30] Hyeon et al. reported that γ-Fe_2O_3 nanocrystals were synthesized by oxidation of the organometallic compound $Fe(CO)_5$ as the precursor with trimethylamine oxides as an oxidant.[28] Yin et al. prepared relatively monodisperse MnO nanocrystals using manganese acetate in a coordinating solvent composed of oleic acid and trioctylamine.[29] The quality of the nanocrystals produced by these nonaqueous solution methods is generally better than that of the nanocrystals synthesized in aqueous solutions.[30] However, to the best of our knowledge, the preparation of Cr_2O_3 nanocrystals by solid thermal decomposition of chromium salts at low temperatures has not been reported so far. Here, we report the synthesis of controlled Cr_2O_3 nanocrystals with mesostructure by the thermal decomposition reaction of chromium salt, which is an inexpensive process to obtain the mesoporous nanocrystals. Meanwhile, we investigated the thermal decomposition of the mixture and the relationship between the structure of the as-synthesized crystallites and the reaction conditions.

Experimental Section

The mesoporous chromium oxide nanocrystals were synthesized using citric acid as a mesopore creating agent by the thermal decomposition of chromium nitrate salt in the autoclave at low temperature. $Cr(NO_3)_3 \cdot 9H_2O$ and citric acid monohydrate (CA) powders were milled separately and then mixed together. The mixture was transferred into an autoclave and heated from 100 °C to 180 °C. The final products were washed with distilled water and dried at 373 K for 12 h.

Infrared spectra of the as-synthesized samples were recorded on a NEXus Fourier transform infrared (FTIR) spectrophotometer using KBr pellets containing 1% wt sample in KBr. Powder X-ray diffraction (XRD) measurement was carried out on a D/MAX-IIIA diffractometer (Japan) with Cu Kα radiation generated at 40 kV, 40 mA at a speed of 0.01°/s, covering 2θ between 2° and 60°. Thermal gravimetric analysis (TGA) and

* To whom correspondence should be addressed. E-mail: zfyancat@hdpu.edu.cn.
† University of Petroleum.
‡ University of Queensland.

10.1021/jp053810b CCC: $33.50
Published on Web 12/08/2005

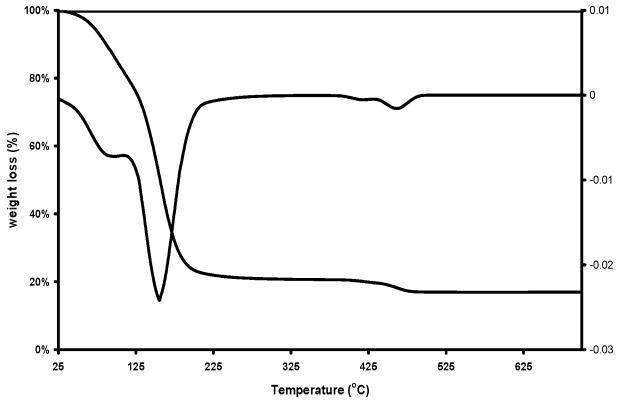

Figure 1. TGA−DTA plot of chromium nitrate.

differential thermalgravimetry (DTG) of the as-synthesized samples were performed at a heating rate of 10 K/min from room temperature to 700 °C in air flow by using a WCT-2 thermal analyzer (Beijing Optical Apparatus Co., China). The surface area, pore volume, and pore size distribution (PSD) of the samples were obtained by nitrogen adsorption−desorption isotherms. N_2 adsorption−desorption isotherms were recorded on a Micromeritics Tristar 2010 nitrogen absorber. The samples were degassed at 373 K for 24 h prior to analysis. The pore size is calculated from the desorption branches of isotherms based on the BJH and HK methods. Transmission electron microscopy (TEM) was conducted on a Philips CM200 microscope with an accelerating voltage 200 kV. The TEM sample was prepared by dipping ultrasonically dispersed Cr_2O_3 particles in ethanol on holey carbon grids. Scanning electron microscopy (SEM) examinations were performed on a JEOL 6300.

Results and Discussion

The TGA and DTG curves of chromium nitrate are shown in Figure 1. There are three different weight loss peaks at the temperature ranges 25−110, 110−217, and 408−490 °C. The first weight loss peak corresponds to the removal of water in the salt. The second is mainly attributed to the decomposition of $Cr(NO_3)_3$ to form Cr_2O_3. The weight loss is about 64%, which is close to the theoretical value. The third one may be ascribed to the removal of the oxygen lattice of Cr_2O_3 due to heating at high temperature. The decomposition reactions of $Cr(NO_3)_3 \cdot 9H_2O$ are as follows[31]

$$Cr(NO_3)_3 \cdot 9H_2O \xrightarrow{30-60\ ^\circ C} Cr(NO_3)_3 \cdot (9-q)H_2O + qH_2O$$

$$Cr(NO_3)_3 \cdot (9-q)H_2O \xrightarrow{60-180\ ^\circ C} Cr^{3+}_{1-x}Cr^{m+}_x O_y(OH)_r(NO_3)_v + HNO_3 + NO + NO_2 + H_2O$$

$$Cr^{3+}_{1-x}Cr^{m+}_x O_y(OH)_r(NO_3)_v \xrightarrow{>120-150\ ^\circ C} Cr_2O_3 + NO + NO_2 + H_2O$$

It is implied that Cr_2O_3 nanocrystals can be obtained at 110−217 °C. So we choose the reaction temperatures at 110−180 °C to synthesize the Cr_2O_3 nanocrystals in this experiment.

Figure 2 shows the XRD patterns of the as-synthesized Cr_2O_3 nanocrystals at different temperatures with a 1:1 molar ratio of $Cr(NO_3)_3 \cdot 9H_2O$-to-CA. The rhombohedra Cr_2O_3 nanocrystals (Figure 2) can be obtained above 130 °C with a precursor-to-CA molar ratio of 1:1. The unit cell parameters and atomic configuration for Cr_2O_3 samples are in good agreement with the known values of well-defined nanocrystals of α-Cr_2O_3,

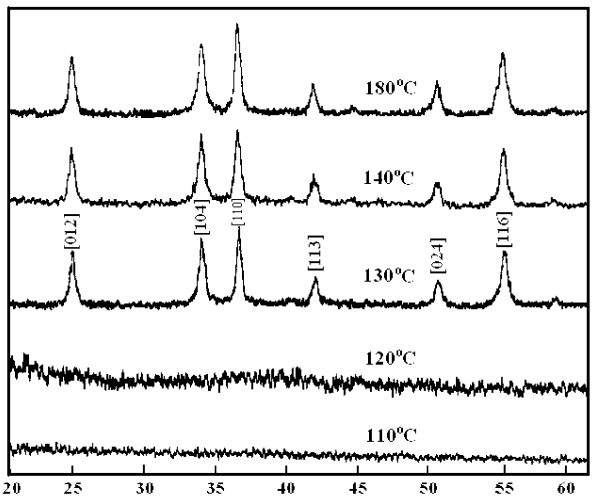

Figure 2. XRD patterns of chromium oxide obtained at different thermal decomposition temperatures for 24 h with the precursor-to-citric acid (CA) molar ratio of 1:1.

which belongs to the $R\bar{3}c$ space group with lattice parameters $a = 4.958$ Å and $c = 13.594$ Å.[32] The crystallite sizes of Cr_2O_3 samples, calculated from the Debye−Scherrer equation, are about 10−15 nm, as also confirmed by the TEM image (Figure 3c). The SEM photographs (parts a and b of Figure 3) reveal the morphology of Cr_2O_3 nanocrystals. Each Cr_2O_3 particle consists of smaller lamellar grains.

The UV−vis spectrum of the Cr_2O_3 nanocrystals is shown in Figure 4. Two UV−vis peaks are observed in the vicinity of 445 (a) and 600 nm (b), corresponding to the $^4A_{2g} \rightarrow {}^4T_{1g}$ and $^4A_{2g} \rightarrow {}^4T_{2g}$ transitions in Cr_2O_3, respectively. The former is characteristic of the Cr^{3+} ions of six-coordinate geometry and the latter of octahedral symmetry.

Figure 5 shows FTIR spectra of the Cr_2O_3 nanocrystals. As seen in Figure 5, a broad band in the 3400−2500 cm^{-1} region corresponds to stretching modes of surface OH groups. The band at 2010−2015 cm^{-1} is ascribed to Cr═O vibration. The bands at ∼1700 cm^{-1}, ∼1680 cm^{-1}, and 1400 cm^{-1} are attributed to hydroxyl groups associated with Cr^{3+} ions occurring in different environments. The 719 cm^{-1} peak is ascribed to the A_{2u} model of Cr_2O_3. A single, strong band at ∼590 cm^{-1} corresponds to the characteristic vibrational mode of a symmetric CrO_6 octahedral of Cr_2O_3 in accordance with the UV−vis spectra analyses of six-coordinate Cr^{3+}.

From the XRD, IR, and UV−vis data, we can conclude that the lattice of α-Cr_2O_3 nanocrystals is built on a hexagonal close-packed (hcp) array of oxygen. The octahedral and tetrahedral sites are located directly above one another in the hcp lattice. The octahedra share faces along a 3-fold axis and are distorted to trigonal antiprisms because of the Cr−Cr repulsion across the shared face. This crystal structure leads to a highly dense structure offering high polarizability, high refractive index, and intense color.[33] The crystal lattice of the Cr_2O_3 sample synthesized is shown in the Figure 6. The character of the atomic structure and electronic configuration is important for the electronic, optical, and magnetic properties of Cr_2O_3.

Figures 7 and 8 show the nitrogen adsorption−desorption isotherms and pore size distribution of Cr_2O_3 nanocrystals obtained from the 1:1 ratio of $Cr(NO_3)_3 \cdot 9H_2O$-to-CA at different thermal decomposition temperatures for 24 h and at 140 °C for different decomposition time. Nitrogen adsorption−desorption isotherms (Figures 7a and 8a) indicate that the isotherms of Cr_2O_3 nanocrystals are of type IV, according to the IUPAC

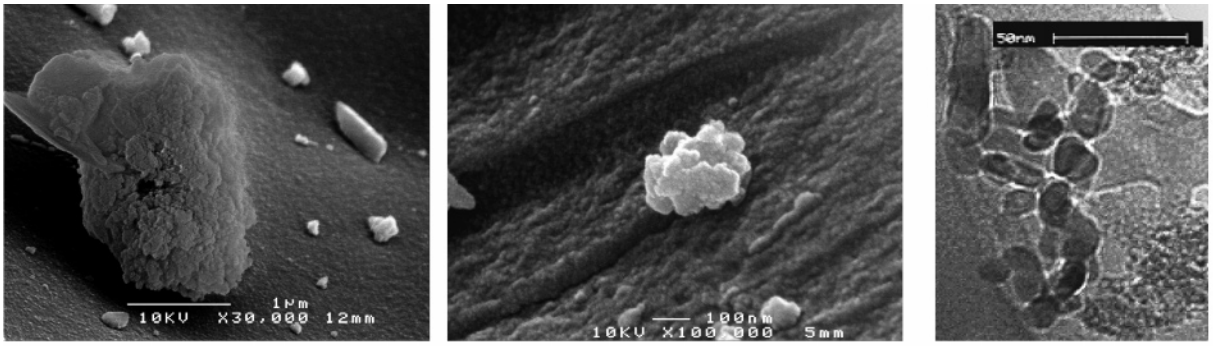

Figure 3. SEM photographs and TEM image of the γ-Cr_2O_3 nanocrystal. (a) SEM image (× 30 000), (b) SEM image (× 100 000), and (c) TEM image.

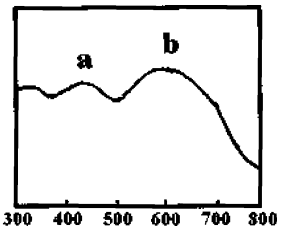

Figure 4. UV−vis spectrum of the Cr_2O_3 nanocrystal.

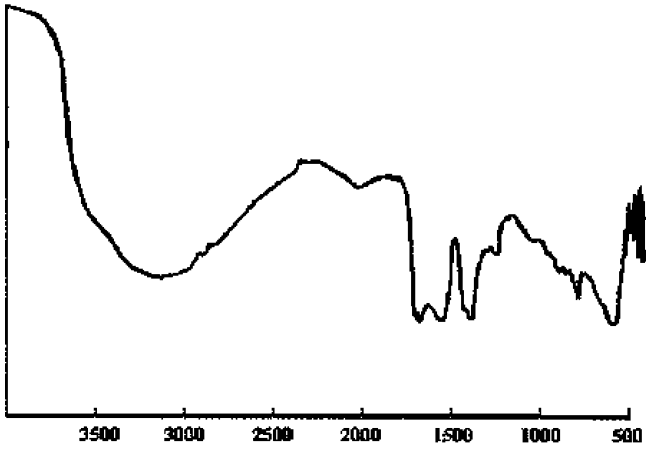

Figure 5. IR spectra of the Cr_2O_3 nanocrystal.

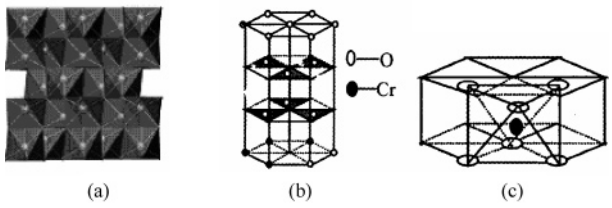

Figure 6. Crystal structure of the α-Cr_2O_3 nanocrystal.

classification, exhibiting the characteristic hysteresis loop of mesoporous materials. This means that the materials obtained by solid thermal decomposition have a mesoporous structure with a wormlike shape. The low-pressure portion of the isotherms is like I type isotherm, indicating the existence of micropores. Therefore, the Cr_2O_3 particles possess mesoporous and microporous dual structures, which are attributed to the removal of CA. Citric acid as an organic additive disperses fully in chromium nitrate. When the mixture is heated, the space occupied by CA remains as pores due to the decomposition of CA. The shape of the pores formed from CA is like vermiform. From Figures 7b and 8b, we can see that the mesopore of chromia prepared with this method possesses bimodal distribution at about 3.5 and 7 nm.

The above results show that nanocrystalline chromium oxide with the mesostructure can be synthesized by the solid decomposition reaction method. In the process, citric acid has an important effect on the mesopore formation of Cr_2O_3. We prepared a Cr_2O_3 sample without CA using the same process and found that the resulting sample has no pores, which indicates that the presence of citric acid in the mixture is critical for the formation of the mesoporous structure. We will investigate the pore formation mechanism and structure of Cr_2O_3 obtained.

The shape, size, and pore structure of nanocrystals can be controlled by the precursor-to-CA ratio, thermal decomposition temperature, and thermal decomposition time. Figure 9 depicts the XRD patterns of Cr_2O_3 samples obtained in the different ratios of metal salt-to-citric acid at 140 °C. It can be seen that amorphous hydrous Cr_2O_3 particles (CrOOH) can be observed in the lower and higher ratios of chromic salt-to-citric acid (1:3, 1:2, and 1:0.3). When the ratio of the precursor to CA was in the medium range such as 1:1 and 1:0.5, the Cr_2O_3 nanocrystals can be obtained. In the decomposition reaction of chromium nitrate in the autoclave, due to the existence of an organic additive, Cr^{3+} ions tended to form entangled cross-links with molten CA[34,35] through hydrogen bonding. The excess of citric acid restrains the condensation of oxonitrates, resulting in the formation of CrOOH particles in the lower ratio of $Cr(NO_3)_3 \cdot 9H_2O$. With the increase in $Cr(NO_3)_3 \cdot 9H_2O$ content, the crystal growth proceeds and the crystals are formed. However, at a higher concentration of $Cr(NO_3)_3 \cdot 9H_2O$, it causes the increase of nucleation to produce a mass of crystal nucleus, which tends to form amorphous Cr_2O_3 particles. We also found that when the reaction temperature was raised or reaction time was prolonged, the crystallite sizes increased accompanied by the broadening of the size distribution (Figures 7b and 8b). From Figure 2, it can be seen that mesoporous Cr_2O_3 crystallites increase with decomposition temperature, which is caused by the crystal growth. Tables 1 and 2 list the surface area, pore volume, and pore diameter of as-synthesized Cr_2O_3 obtained at different thermal decomposition temperatures for 24 h and at 140 °C for different thermal decomposition times, respectively. The surface area and pore volume of Cr_2O_3 samples increase with the rise of temperature and prolongation of time, which is caused by the full decomposition of CA during heating.

In addition, the hydrate water has a crucial effect on crystal growth of Cr_2O_3 from the nucleus clusters. It is found that the crystal nuclei of Cr_2O_3 are formed at a short reaction time from the XRD patterns (Figure 10). With the prolongation of reaction time, to find the low-energy configuration interface from

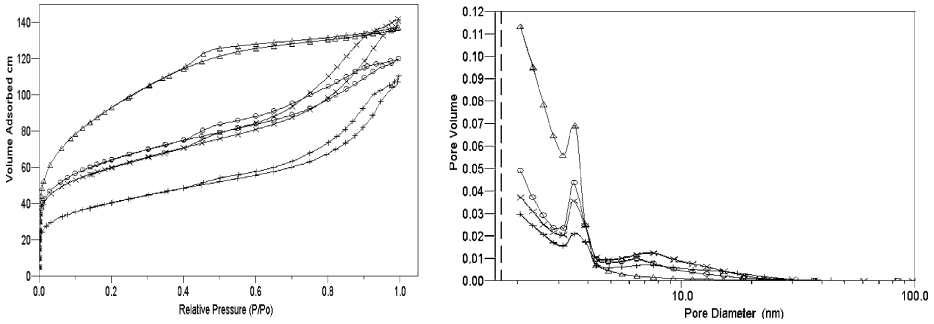

Figure 7. Nitrogen adsorption−desorption isotherms at 77 K and mesoporous size distributions for the Cr_2O_3 samples at different thermal decomposition temperatures when the ratio of $Cr(NO_3)_3 \cdot 9H_2O$-to-CA is 1 (+, 130 °C; ○, 140 °C; ×, 160 °C; Δ, 180 °C).

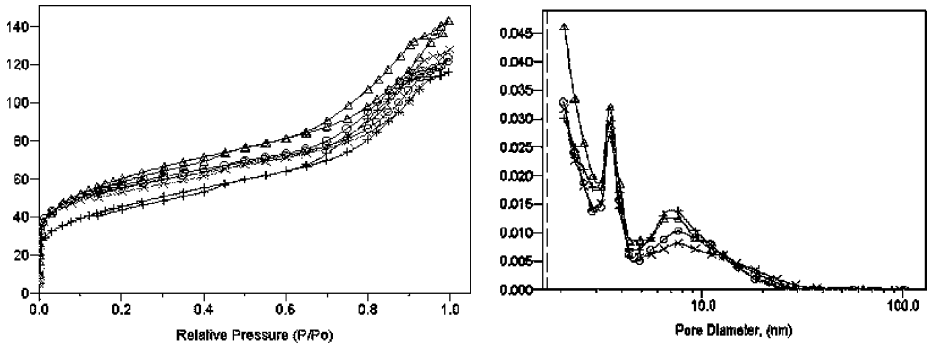

Figure 8. Nitrogen adsorption−desorption isotherms at 77 K and mesopore distributions for the Cr_2O_3 samples at 140 °C for different thermal decomposition times when the ratio of $Cr(NO_3)_3 \cdot 9H_2O$-to-CA is 1 (+, 9 h; ○, 12 h; ×, 36 h; Δ, 72 h).

TABLE 1: Surface Area, Pore Volume, and Diameter of As-Synthesized Cr_2O_3 at Different Temperatures with the $Cr(NO_3)_3 \cdot 9H_2O$ and CA Molar Ratio of 1:1

sample	SA[a] (m^2/g)	SA MS[b] (m^2/g)	SA MI[c] (m^2/g)	PV[d] (cm^3/g)	PV MS[e] (cm^3/g)	PV MI[f] (cm^3/g)	PD[g] (nm)	PD MS[h] (nm)	PD MI[i] (nm)
Cr_2O_3-130	141.4	103.6	29.0	0.171	0.156	0.0135	4.83	6.04	0.64
Cr_2O_3-140	207.2	139.0	52.2	0.185	0.150	0.0657	3.34	4.31	0.70
Cr_2O_3-160	222.0	140.7	60.5	0.220	0.192	0.0628	4.24	5.46	0.60
Cr_2O_3-180	334.0	235.9	13.4	0.212	0.174	0.0843	2.54	2.95	0.71

[a] BET surface area. [b] Surface area of mesopore. [c] Surface area of micropore. [d] Total pore volume. [e] Pore volume of mesopore. [f] Pore volume of micropore. [g] Average pore diameter. [h] Average pore diameter of mesopore. [i] Average pore diameter of micropore.

TABLE 2: Surface Area, Pore Volume and Diameter of As-synthesized Cr_2O_3 at 140 °C for Different Crystallization Times When the Ratio of $Cr(NO_3)_3$ and CA is 1:1

sample	SA[a] (m^2/g)	SA MS[b] (m^2/g)	SA MI[c] (m^2/g)	PV[d] (cm^3/g)	PV MS[e] (cm^3/g)	PV MI[f] (cm^3/g)	PD[g] (nm)	PD MS[h] (nm)	PD MI[i] (nm)
Cr_2O_3-9 h	160.3	121.3	22.6	0.180	0.160	0.0102	4.48	5.54	0.61
Cr_2O_3-12 h	194.1	109.6	56.6	0.191	0.156	0.0273	3.94	5.70	0.62
Cr_2O_3-24 h	207.2	139.0	52.2	0.185	0.150	0.0657	3.34	4.31	0.70
Cr_2O_3-72 h	211.5	141.1	37.7	0.222	0.196	0.0172	4.19	5.57	0.63

[a] BET surface area. [b] Surface area of mesopore. [c] Surface area of micropore. [d] Total pore volume. [e] Pore volume of mesopore. [f] Pore volume of micropore. [g] Average pore diameter. [h] Average pore diameter of mesopore. [i] Average pore diameter of micropore.

nanocrystals and nanocrystal aggregates, the nuclei aggregation will further increase to form nanoparticles. The N_2 isotherms and pore distribution of Cr_2O_3 samples obtained at different thermal decomposition times are shown in Figure 8. It has been seen from Figure 8 and Table 2 that the pore structure and shape have no change but only the size distribution of the samples becomes broader, that is, the particle size of aggregates increases. In the solid thermal decomposition reaction herein, the hydrate water of the mixture provides surface hydroxyls that act as binders, making the nanocrystals aggregate. The aggregation process is slow in the solid reaction. It is easy and effective to control the particle size and distribution during the aggregation process by controlling the water present in the system. The larger the surface hydroxyl density, the larger the particles that form. Meanwhile, the addition of citric acid monohydrate hinders the continuous growth of grain through aggregation of the nanocrystals to form larger particles.

According to the above analyses, the thermal decomposition process of $Cr(NO_3)_3 \cdot 9H_2O$ through the addition of citric acid monohydrate as the mesoporous template agent results in Cr_2O_3 nanocrystals as the building blocks to form a mesoporous wormlike structure of nanoparticles. The formation mechanism of mesoporous Cr_2O_3 nanocrystals is proposed as follows, illustrated in Figure 11. After uniformly mixing with CA,

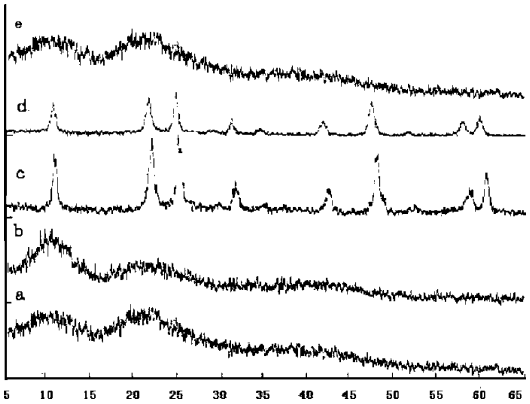

Figure 9. XRD patterns of the mesoporous Cr_2O_3 in the different ratios at 140 °C for 24 h: (a) 1:3, (b) 1:2, (c) 1:1, (d) 1:0.5, and (e) 1:0.3.

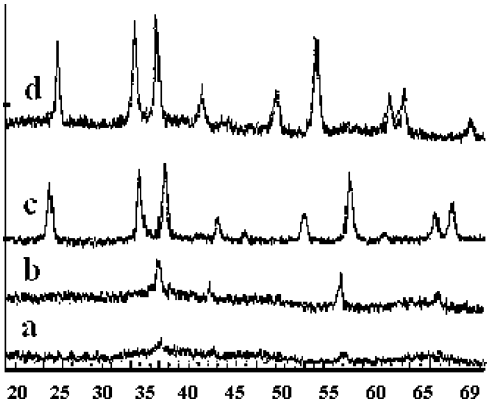

Figure 10. XRD patterns of the mesoporous Cr_2O_3 at 140 °C for different times in the 1:1 ratio of CA and $Cr(NO_3)_3 \cdot 9H_2O$: (a) 12 h, (b) 18 h, (c) 24 h, and (d) 72 h.

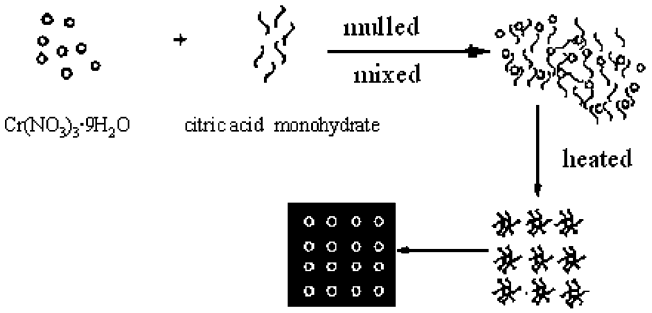

Figure 11. Schematic diagram of the possible mechanism for mesoporous Cr_2O_3 nanoparticles formation.

chromium precursors interact with the CA to form the CA−$Cr(NO_3)_3 \cdot 9H_2O$ composite through hydrogen bonding and electrostatic interaction. Thus, the CA−$Cr(NO_3)_3$ composite decomposes accompanied by the decomposition of the chromium salt and free CA during heating. Since the strength of hydrogen bonding between Cr^{3+} and oxonitrates of chromium and hydroxyl group in CA is not so strong as to restrict the condensation of chromium salt during heating, the Cr_2O_3 network can be formed despite the existence of CA. The introduction of organic additives effectively disperses inorganic species and inhibits the growth of particles. The space occupied with CA creates the disordered wormlike pore of chromium oxide after the thermal decomposition of CA. We also found that there is an optimum amount of critic acid as a dispersed template to stabilize the mesostructure and to achieve maximum porosity.

Conclusions

In summary, mesoporous α-Cr_2O_3 nanocrystals are prepared by a solid thermal decomposition of chromium nitrate with CA as the mesoporous template agent. The as-prepared particles are formed through the aggregation of the primary 3−4 nm nanocrystals and possess mesoporous structure. The XRD, N_2 isotherms, and TEM results suggest that CA has an important effect on the mesopore formation of Cr_2O_3 nanocrystals and acts as a template. The size and pore structure can be tuned by the synthesis conditions, which is achieved by the amount of hydrate water and the addition of citric acid in the mixture system. The binder effect of surface hydroxyl groups is emphasized on the controlled aggregation of metal oxide nanocrystals because only the vicinity of particles can aggregate through surface hydroxyls to form Cr_2O_3 aggregates. The thermal decomposition of citric acid organic molecules makes the space occupied with CA as pores. In addition, such mesoporous Cr_2O_3 nanocrystals will have potential applications in heterogeneous catalysis and we will further investigate the relationships between crystal structure, surface morphology, and catalytic activity.

Acknowledgment. This work is supported by the Petroleum Limited Co. of China. We thank Mr. M. Yan for his assistance on the TEM analysis. Financial support from the Australian Research Council for the ARC Centre for Functional Nanomaterials is also gratefully acknowledged.

References and Notes

(1) Marcus, M. A.; Flood, W.; Stiegerwald, M.; Zahurak, S. F.; Kortan, A. R. *J. Phys. Chem.* **1991**, *95*, 1572.
(2) Boutonnet, M.; Andersson, C.; Larsson, R. *Acta Chem. Scand. A* **1980**, *34*, 639.
(3) Osseo-Asare, K.; Arriagada, F. *J. Colloids Surf.* **1990**, *50*, 321.
(4) Spanhel, L.; Haase, M.; Weller, H.; Henglein, A. *J. Am. Chem. Soc.* **1987**, *109*, 5649.
(5) Abecassis-Wolfovich, M.; Rotter, H.; Landau, M. V.; Korin, E.; Erenburg, A. I.; Mogilyansky, D.; Gartstein, E. *J. Non-Cryst. Solids* **2003**, *318*, 95.
(6) McDaniel, M. P. *Adv. Catal.* **1985**, *33*, 48.
(7) Derossi, S.; Ferraris, G.; Fremiotti, S.; Indovina, V.; Cimino, A. *Appl. Catal., A* **1993**, *106*, 125.
(8) Derossi, S.; Ferraris, G.; Fremiotti, S.; Garrone, E.; Ghiotti, G.; Campa, M. C.; Indovina, V. *J. Catal.* **1994**, *148*, 36.
(9) Cavani, F.; Koutyrev, M.; Trifiro, F.; Bartolini, A.; Ghisletti, D.; Iezzi, R.; Santucci, A.; DelPiero, G. *J. Catal.* **1996**, *158*, 236.
(10) Sohn, J. R.; Ryu, S G.; Kim, H. W. *J. Mol. Catal. Chem.* **1998**, *135*, 99.
(11) Praserthdam, P.; Phungphadung, J.; Tanakulrungsank, W. *Mater. Res. Innovations* **2003**, *7*, 118.
(12) Kobylinski, T. P.; Taylor, B. W. *J. Catal.* **1973**, *31*, 450.
(13) Engweiler, J.; Nickl, J.; Baiker, A.; Kohler, K.; Schlapfer, C. W.; Vonzelewsky, A. *J. Catal.* **1994**, *145*, 141.
(14) Curryhyde, H. E.; Musch, H.; Baiker, A. *Appl. Catal.* **1990**, *65*, 211.
(15) Grzybowska, B.; Sloczynski, J.; Grabowski, R.; Wcislo, K.; Kozlowska, A.; Stoch, J.; Zielinski, J. *J. Catal.* **1998**, *178*, 687.
(16) Lazier, W. A.; Vaughen, J. V. *J. Am. Chem. Soc.* **1932**, *54*, 3080.
(17) Burwell, R. L.; Taylor, H. S. *J. Am. Chem. Soc.* **1936**, *58*, 697.
(18) Burwell, R. L.; Littlewood, A. B.; Cardew, M.; Pass, G.; Stoddart, C. T. H. *J. Am. Chem. Soc.* **1960**, *82*, 6272.
(19) Burwell, R. L.; Taylor, K. C.; Haller, G. L. *J. Phys. Chem.* **1967**, *71*, 4580.
(20) Cross, N. E.; Leach, H. F. *J. Catal.* **1971**, *21*, 239.
(21) Music, S.; Maljkovic, M.; Popovic, S.; Trojko, R. *Croat. Chem. Acta* **1999**, *72*, 789−791.
(22) Tsuzuki, T.; McCormick, P. G. *Acta Mater.* **2000**, *48*, 2795.
(23) Mougin, J.; Le Bihan, T. Lucazeau, G. *J. Phys. Chem. Solids* **2001**, *62*, 553.
(24) Arul Dhas, A.; Koltypin, Y.; Gedanken, A. *Chem. Mater.* **1997**, *9*, 3159.
(25) Kawabata, A.; Yoshinaka, M.; Hirota, K.; Yamaguchi, Q. *J. Am. Ceram. Soc.* **1995**, *78*, 2271.

(26) Hou, B.; Ji, X.; Xie, Y.; Li, J.; Shen, B.; Qian, Y. *Nanostruct. Mater.* **1995**, *5*, 599.

(27) Carlson, E. J.; Armor, J. N.; Cunningham, W. J.; Smith, A. M. U.S. Patent 4828818, 1989.

(28) Hyeon, T.; Lee, S. S.; Park, J.; Chang, Y.; Na, H. B. *J. Am. Chem. Soc.* **2001**, *123*, 12798.

(29) Yin, M.; O'Brien, S. *J. Am. Chem. Soc.* **2003**, *125*, 10180.

(30) Jana, N. R.; Chen, Y. F.; Peng, X. G. *Chem. Mater.* **2004**, *16*, 3931.

(31) Malecki, A.; Gajerski, R.; Labus, S.; et al. *J. Therm. Anal. Calorim.* **2000**, *60*, 17.

(32) McMurdie, H. F.; Morris, M. C.; Evans, E. H.; Paretzkon, B.; Wong-Ng, W.; Zhang, Y.; Hubbard, C. R. *Powder Diffr.* **1987**, *2*, 45.

(33) Vayssieres, L.; Manthiram, A. *J. Phys. Chem. B* **2003**, *107*, 2623.

(34) Liu, G.; Jia, M. J.; Zhou, Z.; Zhang, W. X.; Wu, T. H.; Jiang, D. Z. *Chem. Comm.* **2004**, *14*, 1660.

(35) Takahashi, R.; Sato, S.; Sodesawa, T.; Kawakita, M.; Ogura, M. *J. Phys. Chem. B* **2000**, *104*, 12184.